RESEARCH ARTICLE

The Technique of Thyroid Cartilage Scaffold Support Formation for Extrusion-Based Bioprinting

N. V. Arguchinskaya[1], E. E. Beketov[1]*, A. A. Kisel[1], E. V. Isaeva[1], E. O. Osidak[2], S. P. Domogatsky[2,3], N. V. Mikhailovsky[1], F. E. Sevryukov[1], N. K. Silantyeva[1], T. A. Agababyan[1], S. A. Ivanov[1], P. V. Shegay[4], A. D. Kaprin[4]

[1]A. Tsyb MRRC – Branch of the National Medical Research Radiological Center of the Ministry of Health of the Russian Federation, Obninsk, Russia
[2]Imtek Ltd., Moscow, Russia
[3]Russian Cardiology Research and Production Center Federal State Budgetary Institution, Ministry of Health of the Russian Federation, Moscow, Russia
[4]National Medical Research Radiological Center of the Ministry of Health of the Russian Federation, Obninsk, Russia

Abstract: During biofabrication, a tissue scaffold may require temporary support. The aim of this study was to develop an approach of human thyroid cartilage scaffold temporal support formation. The scaffold 3D-model was based on DICOM images. XY plane projections were used to form scaffold supporting part. To verify the technique, collagen hydrogel was chosen as the main scaffold component. Gelatin was applied for the supporting part. To test the applicability of the approach, a model of thyroid cartilage scaffold with the support was printed. The scaffold corresponded to a given model, although some discrepancy in geometry was observed during verification by computed tomography.

Keywords: Computer-aided design/Computer-aided manufacturing; 3D-bioprinting; Cartilage; Collagen; Gelatin

***Correspondence to:** E. E. Beketov, A. Tsyb MRRC – Branch of the National Medical Research Radiological Center of the Ministry of Health of the Russian Federation, Obninsk, Russia; beketov.ee@yandex.ru

***Received*:** January 18, 2021; **Accepted:** March 5, 2021; **Published Online:** April 12, 2021

Citation: Arguchinskaya NV, Beketov EE, Kisel AA, *et al*., 2021, The Technique of Thyroid Cartilage Scaffold Support Formation for Extrusion-Based Bioprinting. *Int J Bioprint,* 7(2):348. http://doi.org/10.18063/ijb.v7i2.348

1. Introduction

Tissue engineering is based on the use of a scaffold loaded with cells and growth factors. Bioprinting is a good choice for biofabrication of scaffolds with complex or customized geometry. The technology includes not only different types of material dispensing (extrusion-, inkjet-, and laser-based fabrication) but also a number of accompanying techniques, such as the use of medical imaging data (computed tomography [CT] and magnetic resonance imaging) for the scaffold model creation. The ability to reproduce both internal structure and external geometry of the organ or tissue, mimicking native ones is a key advantage of the approach[1,2]. One of the main challenges in bioprinting is related to the materials. Bioprinting requires that a biomaterial provides the scaffold with stability during and after the printing. Furthermore, cell-laden hydrogel should have elasticity in a narrow range that provides not only cell survival but also helps to direct cell differentiation in a certain way[3-5]. It requires the cell-laden material to be both soft for the cells and rigid to maintain the geometry. Sometimes the condition is achievable. Gelation as well as cross-linking processes caused by either ultraviolet (UV)-light, temperature or pH shift take time, and more accurate bioprinting is ensured by hydrogels in the form of high viscous liquid or gel in its early sol-gel stage[6-9]. In both cases, additional material support during biofabrication may be necessary.

Bioprinting is a promising approach for restoration of many types of tissues, including cartilage. The human thyroid cartilage is a good model to verify a new bioprinting technique. The cartilage has a complex geometry with overhanging elements. Its printing process requires the use

of additional support to improve the quality and stability of the scaffold both during and after biofabrication processes. Synthetic polymers such as poly(lactic acid) (PLA) or polycaprolactone (PCL) are widely used[5,10,11]. These components provide a scaffold with necessary stability but do not fully correspond to hydrogel printing conditions (e.g., a temperature). Thus, its application with hydrogels for biofabrication using bioprinting is limited. Another approach related to the use of temporary hydrogel support (e.g., gelatin) still could be applied. In accordance with the technique described in the study, a temporary component is located only in places where the main material needs some prop. Each layer of biomaterial is laid on the previous one consisting either of the same biomaterial or the supporting material. It guarantees stability of the structure during the printing process and formation of required scaffold geometry in the result of biofabrication.

Non-neutralized collagen at the stock concentration was applied as the main cartilage scaffold component. It helped to validate the support performance since no gelation (that increases elasticity of the material) occurred. At the same time, biocompatibility of neutralized collagen was also assessed. The supporting part of the scaffold consists of gelatin, which was a temporary element. The aim of the study was to develop an approach for human thyroid cartilage scaffold temporal support formation, which is applicable in the case of extrusion-based bioprinting with hydrogels.

2. Materials and methods

2.1. 3D-model preparation

The thyroid cartilage model was based on CT images obtained as a part of routing diagnostic procedures. Informed consent was obtained from all patients before the study. Acquisition of CT data was conducted by a multi-detector CT-scanner (Siemens Somatom Emotion 6, Germany). Neck scanning was performed with a slice thickness of 1.25 mm, 0 gantry tilt, and image resolution of 512 × 512 pixels. The acquisition data were stored in DICOM files.

Reconstruction of DICOM images was performed by 3D Slicer 4.10.2 and MeshLab 2016.12. The integrity of a mesh forming the model was checked using Autodesk Meshmixer 3.5.474. The same software was used to estimate the wall thickness of the supporting part of the scaffold. Further processing of the model and its modification for bioprinting was carried out using FreeCAD 0.17. The volume of obtained models was calculated by NewCreatorK 1.57.63. Veusz 3.0.1 was used to visualize the results.

2.2. Hydrogels

Porcine atelocollagen type I (Viscoll, Imtek Ltd, Russia) was used as the main scaffold material. The properties of the material were previously described[12]. Briefly, the material is a soluble collagen fraction obtained by acidic extraction from porcine tendons, purified with a few salt precipitation and ion-exchange chromatography, sterilized by filtration, and stored in lyophilized condition. Collagen gel was prepared by reconstitution of 10 mM acetic acid to a concentration of 80 mg/ml.

Gelatin derived from porcine skin (80–120 g Bloom, Type A, Sigma-Aldrich, cat. no. G6144) was used as temporal material. It was dissolved in distilled water and sterilized by autoclaving (120°C, 1 bar). Gelatin concentration was 12%. At room temperature, the material was in gel state[13].

2.3. 3D-printing procedure

The scaffold was created using extrusion-based print-heads of Rokit *in vivo* 3D-bioprinter (South Korea). Slicing of the model was conducted in NewCreatorK 1.57.63. The scaffold and the support were printed with two 10 ml syringe dispensers. The materials were supplied through 21G needles. The printing was performed on a glass attached to the printing table with magnets. Temperature (23°C) was maintained within the chamber, on the printing table, as well as in the syringes. The main printing options are presented in **Table 1** and were the same for both materials. Immediately after the printing was completed, the object was placed in a cold buffer (80 mM Tris-HCl, PanEco, Russia).

Due to certain mobility of plastic syringes and needles, the centers of printing heads had to be adjusted. For this purpose, the outlines of a 10 mm side square were printed. Previously, one of the outlines had been slightly displaced to improve misalignment visualization. The difference was evaluated by microscopy (Biomed 3, Russia) and ImageJ 1.52.

2.4. CT-verification

The scaffold geometry was verified using CT. The study was performed on Optima CT660 (GE Medical Systems, USA) with 120 kV and 340 mA. The acquisition protocol included the use of 64 detectors, 0.625 mm cut thickness, 0 gantry tilt, and 1.0 s rotation time. Post-processing of CT-acquisition was performed in Advantage Workstation 4.6 (GE Medical Systems, USA). Further procedures were carried out in NewCreatorK 1.57.63 and FreeCAD 0.17.

Table 1. Printing parameters

Parameter	Value
Layer height, μm	386
Input flow, %	150
Fill density, %	66
Infill pattern	concentric
Print speed, mm/s	5.0

When comparing the two models, base levels were set manually. XY planes were matched according to the value of the cut volume (ranging from −2 to +2 mm both for X- and Y-axis). The minimal value was sought. At the chosen point, the difference between the models was estimated.

2.5. Cell culture

The cells were received from Wistar rat rib cartilage (4 days, 8.5 g) following the general recommendations of A Tsyb Minority Recruitment and Retention Committee for bioethics of experimental research on laboratory animals. The primary cell culture was obtained according to Gartland *et al*. protocol[14]. Briefly, a mixture of 0.25% trypsin, 0.2% collagenase II type, and Dulbecco's Modified Eagle's Medium (DMEM) media (these materials were purchased from PanEco, Russia) were used to dissolve the cartilage. After the first step of isolation, the cleaned ribs were left overnight in media with fetal bovine serum (Biosera, France) at 4°C. On the next day, the isolation procedure was repeated, and then the cells were washed by two cycles of precipitation and resuspension. The chondrocytes were cultivated in DMEM (4.5 g/l glucose) with serum, penicillin-streptomycin, and glutamine (both were purchased from PanEco, Russia) at 4°C and 5% CO_2. The cell culture was characterized by Alcian blue stain (Sigma-Aldrich) in accordance with Gosset *et al*. protocol[15]. For the experiment, the second passage was used.

Biocompatibility testing was conducted for neutralized collagen gel with 40 mg/ml concentration (recommended for the study by the manufacturer) in contrast to 80 mg/ml hydrogel that was used to verify the described technique. The neutralization buffer contains 50 mM Tris-HCl and DMEM/F12 medium (pH 8). To examine collagen biocompatibility, 8 × 8 × 0.2 mm scaffolds were printed. Printing parameters and conditions were the same as for the thyroid cartilage scaffold fabrication. The cell-laden scaffolds were incubated in the standard conditions for cell cultures. On the 3rd and 7th days, the tissue scaffolds were analyzed using a Live/Dead assay (Sigma-Aldrich) according to manufacturer protocol. The images were processed using ImageJ 1.52.

2.6. Statistics

Cell viability data were analyzed in R 3.5.3 (2019). The error of cell viability ratio was assessed in accordance with a Poisson distribution. Contingency table and Chi-square test were used to compare cell viability. The difference was considered significant at $P < 0.05$.

3. Results

3.1. Human thyroid cartilage model

The area of interest contouring for each slice was carried out manually (**Figure 1A**). The creation of the 3D model was conducted using context-sensitive smoothing. Subsequent processing was performed in MeshLab. The density of polygonal mesh was reduced, and surface defects were corrected. Thyroid cartilage model (**Figure 1B**) has a dimension of 49.7 × 41.3 × 35.5 mm and consists of 12,712 polygons.

After receiving the mesh type model, it was converted into the solid body in FreeCAD (tolerance for sewing was 0.01). Before further conversion, the model was manually aligned by the base (**Figure 1B**). Locations of the future supports (in places of ledges) are shown in **Figure 1C** and **D**.

3.2. Support formation procedure

The supporting part of the scaffold was located only in places of collagen ledges to optimize the printing process (printing time and amount of material). Thus, the general outline (overall projection) of the entire thyroid cartilage model on the XY-plane was not changed.

A set of scaffold cross-sections was used to create the support. For the preliminary estimation, 2 mm step was chosen (**Figure 2A**). The overall number of slices was 17. Each cross-section was extruded to the base of the model. Thus, a general model for collagen and gelatin was obtained (**Figure 2B**). The support model was obtained by a Boolean operation of subtraction the model of thyroid cartilage from a general model for collagen and gelatin. The complete supporting part of the scaffold (**Figure 2C**) has 23,172 faces and a size of 47.7 × 41.0 × 34.0 mm.

3.2. Influence of cross-section number on the quality of the support

The procedure described above included the use of 17 cross-sections with 2 mm step. The number of slices can vary depending on the given model. The data on the effect

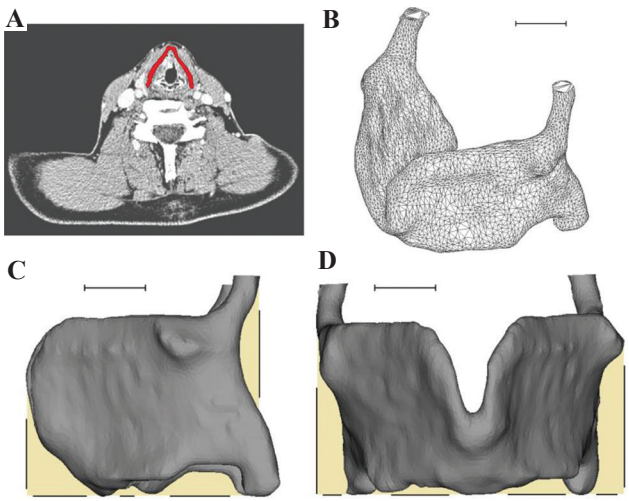

Figure 1. Thyroid cartilage model formation. **(A)** The area of interest at DICOM image (marked in red). **(B)** Model solid body. **(C and D)** Support material location (yellow). Scale bar – 1 cm.

of the cross-section number on the quality of supports obtained are presented in **Figure 3A**.

The volume of the support increases with an increment of slice number. An intermediate value (2 mm) was approved for the study. The use of a smaller step unnecessarily complicates the model increasing the number of polygons (6.81 × 104 for 0.5 mm step), thus, making the process of the support creation more time consuming, necessitating further modification which would toughen both software and hardware.requirements.

Analysis of the effect of each slice (**Figure 3B**) on the formation of the supporting part of the scaffold showed that the greatest increase in the volume of the support is determined by two sets of sections. The first set, which is in the range of 2÷6 mm, is responsible for the base of the support. The second set (12÷24 mm) contributes to the model due to a slope of thyroid cartilage walls. A smaller impact is made by the group of slices in the range of 30÷34 mm. However, they are responsible for an important part of the model which especially needs support. These elements are shown in the upper right part of **Figure 1C**.

3.3. Assessment and modification of the support wall thickness

Further processing of support model included modification of wall thickness. The process of supporting creation (involved subtracting the model of thyroid cartilage from the extruded projections) could lead to the formation of areas with walls thinner than the size of a dispenser nozzle. In this case, a proper slicing procedure (g-code creation) would fail. Ultimately, it would lead to areas where the main material will not have support. In **Figure 4A-C**, such an analysis is presented by means of Meshmixer for the supports with different steps of cross-section (conversation into the solid body was carried out in accordance with standard software parameters). The disagreement of wall thickness with minimal possible value is specific for all variants. To solve this issue, three options were applied in "Accurate mode," as shown in **Table 2**.

The considered parameters refer to the number of voxels used in the courses of primary ("Solid accuracy") and secondary ("Mesh density") approximation of the model, as well as the restriction of minimal thickness.

Table 2. Meshmixer conversation parameters

Procedure	Solid accuracy	Mesh density	Min thickness, mm
1	128	128	0.52
2	128	128	1.03
3	96	512	0.52

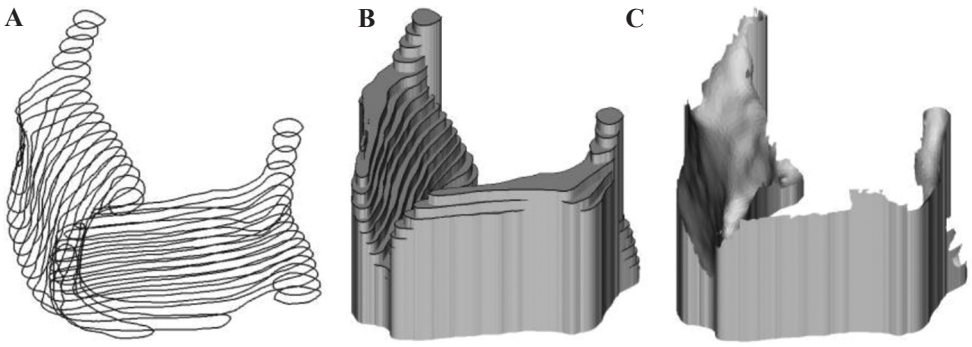

Figure 2. The process of support creation. (**A)** Cross-sections with 2 mm step. **(B)** The volume formed by extruding of each slice to the base. **(C)** The complete support model obtained by subtracting the thyroid cartilage model from the model in **Figure 1(A)**.

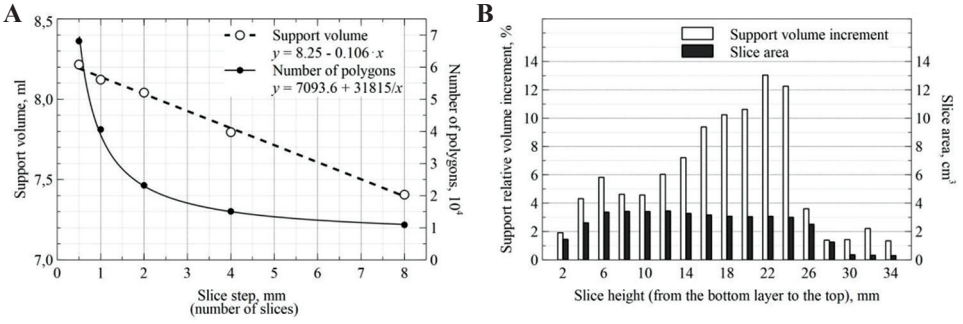

Figure 3. The effect of cross-section number on the quality of supporting part of the scaffold. **(A)** Dependence of the overall volume (model quality) and a number of polygons (model complexity) on the step of the cross-section in the range of 0.5÷8 mm. **(B)** Volume increases for each new slice (from the bottom one) and area of each section for 2 mm step.

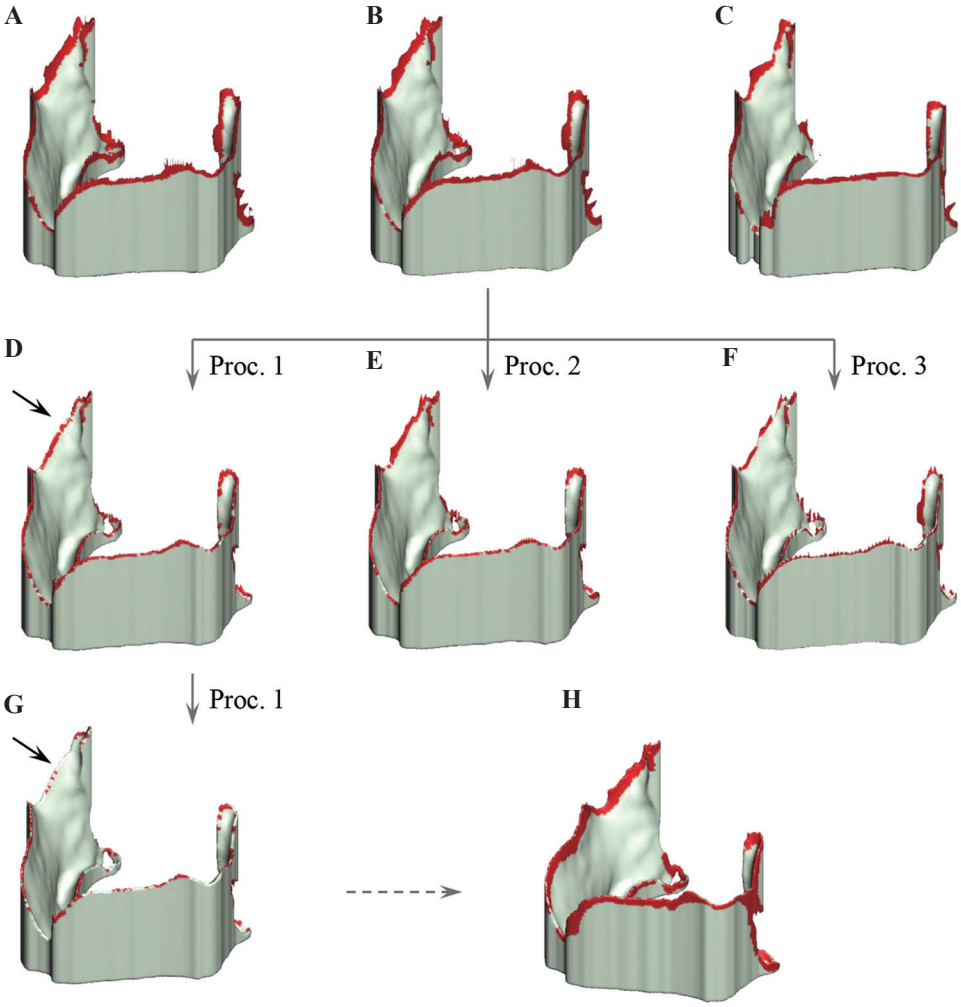

Figure 4. Assessment of wall thickness of the support and optimization options. **(A-C**) Areas with thickness <0.52 cm for options with 0.5, 2.0, and 8 mm slice step, respectively. **(D-G**). The result of procedures 1, 2, and 3 applying the support with 2.0 mm step (b). **(H).** Areas with thickness <1.03 cm for the support with 2.0 mm step underwent double modification according to procedure 1 (g).

The maximal values for the first two parameters were 512. Thus, the used values (96, 128, and 512 units) referred to 19, 25, and 100%. According to the table, procedures 1 and 3 included a minimal thickness value requirement that fitted nozzle diameter (two nozzle diameters in the case of procedure 2). The value of "Solid accuracy" in the case of procedure 3 also fitted diameter of a nozzle (96 units–0.517 mm). The data obtained are presented in **Figure 4D-F**. All approaches have improved wall thickness. Procedure 2 led to undesirable overlap between the support and thyroid cartilage scaffold. Procedure 3 resulted in the unreasonable complication of the model (the number of polygons increased by 15 times). It could be assumed that a slight decrease in "Mesh density" parameter would reduce the complexity of the support but will not contribute to the issue of wall thickness. Another optimization option was considered. Procedure 1 was reapplied (Figure 4G). The effect (the most pronounced change is shown by arrows) was satisfactory and did not result in complication of the model.

It should be noted that all these procedures were not accompanied by the change in volume of the support. The decrease in this parameter for **Figure 4D-G** was 0.90, 0.80, 0.95, and 1.10% of the initial model (**Figure 4B**), respectively.

Depending on printing parameters, the problem of excessively thin walls may be almost unsolvable. The areas of wall thickness model of <1.03 mm are shown in **Figure 4H**. These data are important for printing of the scaffold with supports on a small scale (e.g., 1:2), or in the case of non-standard printing parameters (e.g., material output, and fill density). Both events were investigated in this study. An additional application of the procedures for wall thickness optimization was impossible since this would inevitably entail critical changes in the geometry of the support.

3.5. 3D bioprinting

Since extrusion-based bioprinting with mechanical material supply does not provide instant pressure relief and subsequent sharp pressure increase in the syringes when the dispenser change takes place (in contrast to pneumatic dosing), the formation of each new layer requires preliminary normalization of the parameter. For these purposes, next to the main object, an additional element was printed (in **Figure 5A** and **B** on the left). During its formation, the pressure in the syringe was increased and by the time the scaffold was printed, it reached the required value.

The decrease in material retraction frequency during non-printing motions (both with gelatin or collagen) was minimized using a concentric filling pattern. Preliminary material testing showed that 150% material output and layer height at the level of 75% of nozzle diameter (386 μm in the case of 21G needles) were appropriate printing parameters for both materials. Filling density was set at 66% (corresponding to 99% filling for 150% material output).

The described approach was verified by printing a cell-free scaffold of thyroid cartilage at 1:2 scales. The printing was conducted by two dispensers containing collagen, and gelatin. The complete scaffold is shown in **Figure 5B**. The scaffold was printed twice to confirm the quality of the support. The printed scaffold corresponds to the given thyroid cartilage model on the whole. Gelatin support was well visualized. Certain defects in the design of the scaffold occur due to the small scale and can be eliminated by printing in full-size mode. For further procedures, the object was placed in the cold buffer bath.

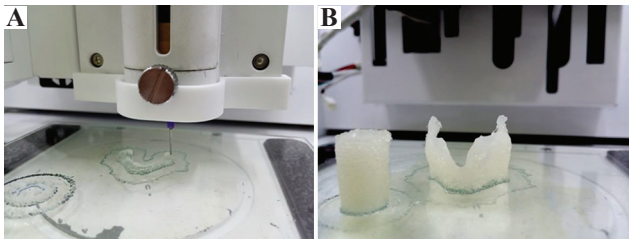

Figure 5. The thyroid cartilage scaffold with the support. **(A)** In the beginning of biofabrication: The white component was collagen, while the transparent component was gelatin**. (B)** Immediately after the printing: On the left side, the additional printing element, required for normalization of pressure in a syringe after changing the dispenser at each new layer.

3.6. Geometry verification

The geometry of the printed scaffold with the support was verified using CT (**Figure 6A**). Since incubation buffer and collagen (as well as gelatin) have almost the same density, the solution was removed before CT-verification. Some geometry-related discrepancy with the input model (also general for collagen and gelatin) was observed. The possible reasons for this were half-scale object printing, processes of material fluidity, and drying process during and after the printing (including the time before the CT-scanning). In respect of the total volume, the printed object exceeded the input model by 10.4% (18.013 cm^3 vs. 16.314 cm^3). The printed object had the redundant volume at the level of 24.0 % (**Figure 6C**) and the missing volume of 13.6% (**Figure 6D**). The conforming volume (for the model and printed object, **Figure 6B**) was 86.4%.

3.7. Biocompatibility

High cell survival was observed on the 3rd day of scaffold incubation (**Figure 7A**). There were 88.1 ± 5.3% of living cells according to the Live/Dead assay. In 4 days (**Figure 7B**), cell viability increased up to 94.5 ± 5.2%. The difference was significant, according to Chi-square test. Thus, the used biomaterial provides the necessary level of biocompatibility for cell survival and proliferation.

4. Discussion

In the literature, there is a significant number of studies on the restoration of cartilage using hydrogel-based scaffolds. However, they are mainly related to objects up to 0.5 mm in height. There were few studies aimed at creating complete cartilage scaffolds[16,17]. Sun *et al*.[18] fabricated scaffolds which could be applied for treating thyroid cartilage injuries using low-temperature deposition technology with hydroxyapatite and chitosan.

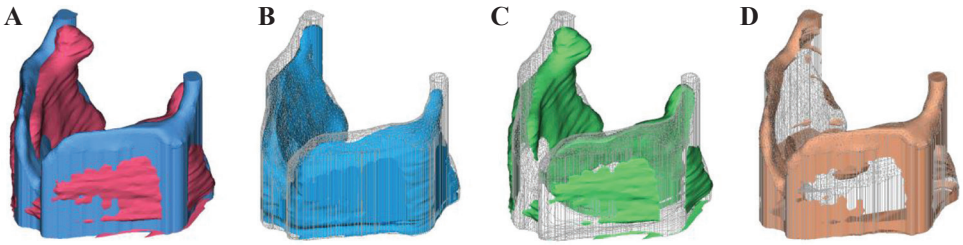

Figure 6. Thyroid cartilage scaffold with the support. (**A**) The input model (marked in blue) and the printed object CT-reconstruction (red). (**B**) The conforming volume (blue). **(C)** The redundant volume (green). **(D)** The missing volume (orange).

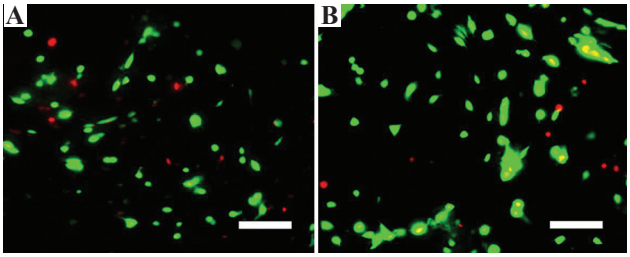

Figure 7. Estimation of viability rat chondrocytes in collagen scaffold through staining **(A)** On the 3rd and **(B)** 7th days of incubation. The green indicates live cells, while the red indicates dead cells. Composite images were made of 10 layers. Scale bar – 100 μm.

This method provides well-formed porous structures, large surface area and space for cell attachment, growth, and proliferation. Moreover, larynx and trachea scaffolds made of polypropylene mesh covered with collagen sponge have already been used clinically[19]. The technology involves the use of a tube-shaped frame (made of polypropylene mesh), as well as polypropylene support ring embedded in it to provide rigidity to the structure. The inner and outer surfaces of the tubes were coated with collagen. Our results on collagen biocompatibility testing confirm suitability of collagen as a substrate/scaffold for cell proliferation.

Since both technologies described above are related to the acellular scaffold type, they could not be directly compared with the method described in the study. The technique which is closest to our approach was described by Hinton *et al*.[20]. They used freeform reversible embedding of suspended hydrogels (FRESH). Based on the technique, printing hydrogel was embedded in a secondary hydrogel, which serves as temporary thermoreversible and biocompatible support. 3D-imprints of alginate, fibrin, matrigel, and collagen were obtained. The method was later improved to ensure higher printing accuracy[21]. Other similar techniques have been described by Bhattacharjee *et al*.[22] and Wu *et al*.[23]. An alternative approach for biofabrication of a scaffold with high complexity in its geometry is related to the use of reverse strategy: Placement of sacrificial material in main material. Basically, such constructions serve as an additional means of forming hollow channels[24-28]. However, when the geometry is complicated, the use of an additional custom-shaped mold may be required in order to form the scaffold, and bioprinting is used only to create the internal structure of the scaffold[29].

Most of the biomaterials used for bioprinting are usually soft (resulting in fragility of the printed scaffolds); therefore, there is a high probability of deformation of the material under its own weight. For the formation of an elastic filament during the material extrusion, a stage of polymerization and/or cross-linking is urgent. Depending on the design of the study, internal structure and geometry of a scaffold, the polymerization and/or cross-linking occur before or during bioprinting, or even after the formation of the whole scaffold. The guided polymerization and/or cross-linking of the biomaterial are influenced by different physical and chemical factors: UV, temperature, ion concentration, pH, etc. Collagen is a fibrillar protein comprising of connective tissue (tendon, bone, cartilage, dermis, etc.). Collagen type I is characterized by high affinity to the cells and lack of species specificity[1,30]. The material provides cell adhesion, migration, proliferation, and differentiation. As a component of extracellular matrix, collagen ensures the rigidity and integrity of a tissue[2]. However, collagen itself has weak mechanical properties and a high rate of biodegradation. The native way of collagen polymerization is a shift in temperature (increase) and pH (increase)[31]. Another option suggests inverse pH change (decrease), but it will result in low cell viability[32,33]. The applicability of additional chemical cross-linking with genipin[34], tannic acid[35], glutaraldehyde[36], and dialdehyde starch[37] has been shown. Drzewiecki *et al*. described the use of photocuring collagen methacrylamide as a bio-ink (cell-laden biomaterial applicable for bioprinting)[38]. Another option is riboflavin that provides the formation of covalent crosslinks in collagen[39]. In the present study, no forced cross-linking and high concentration of the material were used to increase stiffness of the scaffold.

In our study, gelatin served as the supporting material. Gelatin is a collagen hydrolysate. and has the same amino acid composition[40]. Unlike collagen, gelatin is soluble in water. In tissue engineering, gelatin is used as sacrificial material that could be easily removed at 37°C (standard temperature for cell culture and tissue scaffolds incubation). In general, gelatin is not characterized by antigenic and immunogenic properties[41]. It is relatively cheap, making it a very attractive material for 3D-bioprinting. For many years, its reversible "Sol-Gel" transition has been used for temporal (sacrificial) scaffold elements. Recently, the use of a commercial product called Pluronic F-127 has become extensive for this purpose[31,42,43]. The material was also adapted to form macropores in a scaffold[31]. Fitzsimmons *et al*.[42] showed that Pluronic F-127 is superior to gelatin as a sacrificial material for creating vascularized tissues. Both gelatin and Pluronic F-127 have high printability and ease of removal. Filament printed with Pluronic F-127 has higher spatial resolution, greater uniformity, and modulus of elasticity than the one of gelatin[42]. At the same time, the use of Pluronic F-127 strictly requires incubation at low temperature (e.g., 4°C) after the printing to complete its removal from a scaffold[44], while gelatin can easily melt at standard temperature (37°C). Gelatin could be considered as a more affordable material and thus, the first choice for

any study. In any case, both materials could be applied to the technique described in the study.

The used concentration of low-Bloom gelatin (12%) provided rapid "Sol-Gel" transition at room temperature. In case of higher Bloom value (e.g., 300 g Bloom) or lower temperature of the printing table, less concentrated gelatin should be applied. In the present study, sterilization of gelatin was achieved by autoclaving. According to our data, this step does not significantly affect gelatin ability of "Sol-Gel" transition.

The current stage in the development of bioprinting is closely related to hydrogels. A number of biologically inert synthetic polymers can be considered the heritage of conventional 3D-printing. They have been used both as a temporary supporting part[45] or a constant supporting element of a scaffold[5,10,11]. However, since its extrusion temperature is much higher than the one appropriate for cells and hydrogel (in gel state), the use of PLA, PVA (both 180–200°C), and PCL (60–120°C) could not be considered the first choice for bioprinting (in contrast to other tissue engineering approaches). The exception is its use for a base layer of a scaffold.

The approach proposed in the study is based on the use of original model cross-sections. Unlike other studies, the technique considers printing process optimization, specifically, and printing time. The method showed its applicability in the case of complex geometry. Application of this approach requires validation of printing parameters, such as nozzle diameter, filling pattern, filling percentage, as well as retraction of related settings. It has been shown that creation of the support from a cross-section set with a rare slice step could reduce its quality, and an increase of the parameter leads to unreasonable complication of the model. Similarly, the process of wall thickness modification should take into consideration should be well-balanced.

In the experiment, we found that printing duration was one of the main issues. The formation of the human thyroid cartilage scaffold in scale 1:2 took about 1.5 h to complete (excluding preparatory procedures). Printing of the full-sized scaffold would take over 5 h. To solve this problem, it is advisable to use bigger needles (e.g., 18G vs. 21G needles used in the study). However, along with the acceleration of the printing process (up to 2.5 h); It will irreversibly decrease the scaffold quality. The issue of printing time is related to another one related to CT-verification. The problem of scaffold drying in the course of bioprinting arises in many current bioprinters models. Biofabrication of half- or full-scale objects requires the possibility to control the chamber humidity. Although the use of FRESH technique may be able to offer a solution, this approach has its own limitations and is not applicable in many bioprinters.

Another challenge of the research was related to geometry verification. In the course of CT-verification, the similar density levels of collagen and surrounding media (buffer) posed a problem to geometry verification. To verify scaffold geometry, two options were possible. The first one is related to the use of contrast agent whereas the other one required media (buffer) removal. Thus, in future studies, the use of an additional high-density scaffold component is required as it could distinguish the scaffold outline and thereby provide more accurate geometry verification.

5. Conclusion

The proposed technique for bioprinting of tissue scaffolds with complex geometry using temporal support was verified. The approach is applicable in hydrogel-based biofabrication using a two-dispenser bioprinter. This method is not limited for use with human thyroid cartilage; it can be applied to other types of cartilage as well as other tissue types.

Conflict of Interest

No potential conflict of interest was reported by the authors.

References

1. Ng WL, Chua CK, Shen YF, 2019, Print Me An Organ! Why We Are Not There Yet. *Prog Polym Sci*, 97:101145. https://doi.org/10.1016/j.progpolymsci.2019.101145
2. Lee JM, Ng WL, Yeong WY, 2019, Resolution and Shape in Bio-Printing: Strategizing Towards Complex Tissue and Organ Printing. *Appl Phys Rev*, 6:11307. https://doi.org/10.1063/1.5053909
3. Engler AJ, Sen S, Sweeney HL, *et al*., 2006, Matrix Elasticity Directs Stem Cell Lineage Specification. *Cell*, 126:677–89. https://doi.org/10.1016/j.cell.2006.06.044
4. Hadden WJ, Young JL, Holle AW, *et al*., 2017, Stem Cell Migration and Mechanotransduction on Linear Stiffness Gradient Hydrogels. *Proc Natl Acad Sci*, 114:5647–52. https://doi.org/10.1073/pnas.1618239114
5. Ke D, Yi H, Est-Witte S, *et al*., 2019, Bioprinted Trachea Constructs With Patient-Matched Design, Mechanical and Biological Properties. *Biofabrication*, 12:15022. https://doi.org/10.1088/1758-5090/ab5354
6. Ouyang L, Highley CB, Sun W, *et al*., 2017, A Generalizable Strategy for the 3D Bioprinting of Hydrogels from Non Viscous Photo-Crosslinkable Inks. *Adv Mater*, 29: 1604983. https://doi.org/10.1002/adma.201604983
7. Kim SH, Yeon YK, Lee JM, *et al*., 2018, Publisher Correction: Precisely Printable and Biocompatible Silk Fibroin Bio-Ink for Digital Light Processing 3D Printing, *Nat Commun*, 9:2350.

https://doi.org/10.1038/s41467-018-04517-w

8. Onofrillo C, Duchi S, O'Connell CD, *et al*., 2018, Biofabrication of Human Articular Cartilage: A Path towards the Development of a Clinical Treatment. *Biofabrication*, 10:45006. https://doi.org/10.1088/1758-5090/aad8d9
9. Kajave NS, Schmitt T, Nguyen TU, *et al*., 2020, Dual Crosslinking Strategy to Generate Mechanically Viable Cell-Laden Printable Constructs using Methacrylated Collagen Bio-Inks. *Mater Sci Eng C Mater Biol Appl*, 107:110290. https://doi.org/10.1016/j.msec.2019.110290
10. Park JH, Hong JM, Ju YM, *et al*., 2015, A Novel Tissue-Engineered Trachea With a Mechanical Behavior Similar to Native Trachea. *Biomaterials*, 62:106–15. https://doi.org/10.1016/j.biomaterials.2015.05.008
11. Gao M, Zhang H, Dong W, *et al*., 2017, Tissue-Engineered Trachea from a 3D-Printed Scaffold Enhances Whole-Segment Tracheal Repair. *Sci Rep*, 7:5246. https://doi.org/10.1038/s41598-017-05518-3
12. Osidak EO, Karalkin PA, Osidak MS, *et al*., 2019, Viscoll Collagen Solution as a Novel Bio-Ink for Direct 3D Bio-Printing. *J Mater Sci Mater Med*, 30:31.
13. Yang LJ, Lin WZ, Yao TJ, *et al*., 2003, Photo-Patternable Gelatin as Protection Layers in Low-Temperature Surface Micromachinings. *Sens Actuators A Phys*, 103:284–9. https://doi.org/10.1016/s0924-4247(02)00338-2
14. Gartland A, Mechler J, Mason-Savas A, *et al*., 2005, *In Vitro* Chondrocyte Differentiation using Costochondral Chondrocytes as a Source of Primary Rat Chondrocyte Cultures: An Improved Isolation and Cryopreservation Method. *Bone*, 37:530–44. https://doi.org/10.1016/j.bone.2005.04.034
15. Gosset M, Berenbaum F, Thirion S, *et al*., 2008, Primary Culture and Phenotyping of Murine Chondrocytes. *Nat Protoc*, 3:1253–60. https://doi.org/10.1038/nprot.2008.95
16. Apelgren P, Amoroso M, Lindahl A, *et al*., 2017, Chondrocytes and Stem Cells in 3D-Bioprinted Structures Create Human Cartilage *In Vivo*. *PLoS One*, 12:e0189428. https://doi.org/10.1371/journal.pone.0189428
17. Jung CS, Kim BK, Lee J, *et al*., 2017, Development of Printable Natural Cartilage Matrix Bio-Ink for 3D Printing of Irregular Tissue Shape. *Tissue Eng Regen Med*, 15:155–62. https://doi.org/10.1007/s13770-017-0104-8
18. Sun N, Shib T, Fanc Y, *et al*., 2018, Experimental Study on 3D Chi-Hap Scaffolds for Thyroid Cartilage Repairing. *IOP Conf Ser Mater Sci Eng*, 301:012018. https://doi.org/10.1088/1757-899x/301/1/012018
19. Omori K, Tada Y, Suzuki T, *et al*., 2008, Clinical Application of *In Situ* Tissue Engineering using a Scaffolding Technique for Reconstruction of the Larynx and Trachea. *Ann Otol Rhinol Laryngol*, 117:673–8. https://doi.org/10.1177/000348940811700908
20. Hinton TJ, Jallerat Q, Palchesko RN, *et al*., 2015, Three-Dimensional Printing of Complex Biological Structures by Freeform Reversible Embedding of Suspended Hydrogels. *Sci Adv*, 1:e1500758. https://doi.org/10.1126/sciadv.1500758
21. Lee A, Hudson AR, Shiwarski DJ, *et al*., 2019, 3D Bioprinting of Collagen to Rebuild Components of the Human Heart. *Science*, 365:482–7.
22. Bhattacharjee T, Zehnder SM, Rowe KG, *et al*., 2015, Writing in the Granular Gel Medium. *Sci Adv*, 1:e1500655. https://doi.org/10.1126/sciadv.1500655
23. Wu W, DeConinck A, Lewis JA, 2011, Omnidirectional Printing of 3D Microvascular Networks. *Adv Mater*, 23:H178–83. https://doi.org/10.1002/adma.201004625
24. Lee W, Lee V, Polio S, *et al*., 2010, On-Demand Three-Dimensional Freeform Fabrication of Multi-Layered Hydrogel Scaffold with Fluidic Channels. *Biotechnol Bioeng*, 105:1178–86. https://doi.org/10.1002/bit.22613
25. Miller JS, Stevens KR, Yang MT, *et al*., 2012, Rapid Casting of Patterned Vascular Networks for Perfusable Engineered Three-Dimensional Tissues. *Nat Mater*, 11(9):768–74. https://doi.org/10.1038/nmat3357
26. Bertassoni LE, Cecconi M, Manoharan V, *et al*., 2014, Hydrogel Bioprinted Microchannel Networks for Vascularization of Tissue Engineering Constructs. *Lab Chip*, 14:2202–11. https://doi.org/10.1039/c4lc00030g
27. Lee VK, Kim DY, Ngo H, *et al*., 2014, Creating Perfused Functional Vascular Channels using 3D Bio-Printing Technology. *Biomaterials*, 35:8092–102. https://doi.org/10.1016/j.biomaterials.2014.05.083
28. Lee VK, Lanzi AM, Haygan N, *et al*., 2014, Generation of Multi-Scale Vascular Network System within 3D Hydrogel using 3D Bio-Printing Technology. *Cell Mol Bioeng*, 7:460–72. https://doi.org/10.1007/s12195-014-0340-0
29. Skylar-Scott MA, Uzel SG, Nam LL, *et al*., 2019, Biomanufacturing of Organ-Specific Tissues with High Cellular Density and Embedded Vascular Channels. *Sci Adv*, 5:eaaw2459.

https://doi.org/10.1126/sciadv.aaw2459

30. Dong C, Lv Y, 2016, Application of Collagen Scaffold in Tissue Engineering: Recent Advances and New Perspectives. *Polymers*, 8:42. https://doi.org/10.3390/polym8020042
31. Lee J, Kim G, 2018, Three-Dimensional Hierarchical Nanofibrous Collagen Scaffold Fabricated using Fibrillated Collagen and Pluronic F-127 for Regenerating Bone Tissue. *ACS Appl Mater Interfaces*, 10:35801–11. https://doi.org/10.1021/acsami.8b14088
32. Doyle AD, 2016, Generation of 3D Collagen Gels with Controlled Diverse Architectures. *Curr Protoc Cell Biol*, 72:10.20.1–16.
33. Naciri M, Kuystermans D, Al-Rubeai M, 2008, Monitoring pH and Dissolved Oxygen in Mammalian Cell Culture Using Optical Sensors. *Cytotechnology*, 57:245–50. https://doi.org/10.1007/s10616-008-9160-1
34. Kim YB, Lee H, Kim GH, 2016, Strategy to Achieve Highly Porous/Biocompatible Macroscale Cell Blocks, using a Collagen/Genipin-Bioink and an Optimal 3D Printing Process. *ACS Appl Mater Interfaces*, 8:32230–40. https://doi.org/10.1021/acsami.6b11669
35. Lee J, Yeo M, Kim W, *et al*., 2018, Development of a Tannic Acid Cross-Linking Process for Obtaining 3D Porous Cell-Laden Collagen Structure. *Int J Biol Macromol*, 110: 497–503. https://doi.org/10.1016/j.ijbiomac.2017.10.105
36. Peng YY, Glattauer V, Ramshaw JA, 2017, Stabilisation of Collagen Sponges by Glutaraldehyde Vapour Crosslinking, *Int J Biomater*, 2017:8947823. https://doi.org/10.1155/2017/8947823
37. Mu C, Liu F, Cheng Q, *et al*., 2010, Collagen Cryogel Cross-Linked by Dialdehyde Starch. *Macromol Mater Eng*, 295:100–7. https://doi.org/10.1002/mame.200900292
38. Drzewiecki KE, Malavade JN, Ahmed I, *et al*., 2017, A Thermoreversible, Photocrosslinkable Collagen Bio-Ink for Free-Form Fabrication of Scaffolds for Regenerative Medicine, *Technology* (*Singap World Sci*), 5:185–95. https://doi.org/10.1142/s2339547817500091
39. Diamantides N, Wang L, Pruiksma T, *et al*., 2017, Correlating Rheological Properties and Printability of Collagen Bioinks: The Effects of Riboflavin Photocrosslinking and pH. *Biofabrication*, 9:34102. https://doi.org/10.1088/1758-5090/aa780f
40. Shi W, Sun M, Hu X, *et al*., 2017, Structurally and Functionally Optimized Silk-Fibroin-Gelatin Scaffold Using 3D Printing to Repair Cartilage Injury *In Vitro* and *In Vivo*. *Adv Mater*, 29: 1701089. https://doi.org/10.1002/adma.201701089
41. Setayeshmehr M, Esfandiari E, Rafieinia M, *et al*., 2019, Hybrid and Composite Scaffolds Based on Extracellular Matrices for Cartilage Tissue Engineering. *Tissue Eng Part B Rev*, 25:202–24. https://doi.org/10.1089/ten.teb.2018.0245
42. Fitzsimmons R, Aquilino MS, Quigley J, *et al*., 2018, Generating Vascular Channels within Hydrogel Constructs using an Economical Open-Source 3D Bioprinter and Thermoreversible Gels. *Bioprinting*, 9:7–18. https://doi.org/10.1016/j.bprint.2018.02.001
43. Kolesky DB, Truby RL, Gladman AS, *et al*., 2014, 3D Bioprinting of Vascularized, Heterogeneous Cell-Laden Tissue Constructs. *Adv Mater*, 26:3124–30. https://doi.org/10.1002/adma.201305506
44. Paulsen SJ, Miller JS, 2015, Tissue Vascularization through 3D Printing: Will Technology Bring us Flow? *Dev Dyn*, 244:629–40. https://doi.org/10.1002/dvdy.24254
45. Kim HD, Lee Y, Kim Y, *et al*., 2017, Biomimetically Reinforced Polyvinyl Alcohol-Based Hybrid Scaffolds for Cartilage Tissue Engineering. *Polymers*, 9:655. https://doi.org/10.3390/polym9120655